A Hybrid Coupler for 6.78MHz Desktop Wireless Power Transfer Applications with Stable Open-loop Gain

Chen, Xu; Yu, Shengbao; Song, Shuchao; Li, River T. H. ; Yang, Xiaobo; Zhang, Zhe

Published in:
IET Power Electronics

Link to article, DOI:
10.1049/iet-pel.2018.6199

Publication date:
2019

Document Version
Peer reviewed version

A Hybrid Coupler for 6.78MHz Desktop Wireless Power Transfer Applications with Stable Open-loop Gain

Xu Chen [1], Shengbao Yu [1*], Shuchao Song [1], River T. H. Li [2], Xiaobo Yang[3], Zhe Zhang [4]

[1]College of Instrumentation and Electrical Engineering; Key Laboratory of Earth Information Detection Instrumentation, Jilin University, Changchun 130026, Jilin Province, China
[2] Hong Kong Applied Science and Technology Research Institute Co. Ltd, Hong Kong, China
[3] ABB (China) Limited, Beijing 100015, China
[4] Department of Electrical Engineering, Technical University of Denmark, 2800 Kongens Lyngby, Denmark
[*] yushengbao@jlu.edu.cn

Abstract: The open-loop gain of capacitive power transfer (CPT) circuit, especially for applications like wireless charging of laptop or keyboard, is sensitive to the changes of coupling capacitance, which makes the regulating of output voltage and output power difficult. Hybrid coupler has been proved to be able to combine the advantages of both inductive power transfer (IPT) and capacitive power transfer. In this paper, a hybrid coupler is designed with the aim of keeping a stable open-loop gain when the coupling capacitance changes. The structure as well as the operation principles of the hybrid coupler is explained firstly. Then, the open-loop gains of CPT, IPT and hybrid wireless power transfer (HWPT) are derived and followed by a simplified design guideline of the whole HWPT system using the proposed hybrid coupler. Finally, the proposed coupler is verified with a 40W, 6.78MHz experimental prototype.

1. Introduction

Wireless power transfer (WPT) is an attractive research topic for its advantages in convenience, safety and neatness compared with conventional wired power transfer. It is also a challenging research topic due to its unique system configuration especially in aspects like reliability, efficiency, robustness, EMI and etc. Depending on the medium used, a WPT system can either be inductive power transfer (IPT), which uses magnetic field to transfer power [1]-[3], or capacitive power transfer (CPT), which uses electric field to transfer power [4]-[6].

For the low power application like wireless charging of computer and tablet, most of the research work so far uses IPT methods. Two standards can be found about inductive power transfer in this application, 'Qi' standard [7] and 'A4WP' standard [8]. The main difference of the two standards is switching frequency. 'Qi' standard IPT system operates between 110-205kHz, while those follow 'A4WP' standard operates at around 6.78MHz (6.765-6.795MHz) [9]. Here, 6.78MHz is one of the industrial, scientific and medical (ISM) radio bands that can be used free of license. Although 6.78MHz IPT methods can be used for desktop wireless power transfer, it has some limitations. For example, it's difficult to design an efficient power converter operating at multi-megahertz, W. Chen investigated the design challenges of 25W GaN based class-E inverter capable of operating at 13.56MHz [10]. It's also difficult to design and fabricate a coupling coil as big as the bottom surface of receiver devices (e.g. the bottom surface of laptop) because an IPT coil normally needs magnetic cores or magnetic sheets to shield the high frequency field and protect the electronic devices inside the laptop from been affected by charging fields. To the author's knowledge, no rigid magnetic core is available with such big area. Soft magnetic sheets like IFL12 might be used, but its price is too high to be accepted compared with the price of electronic device itself. The safety concerns of high frequency leakage magnetic field around desktop is also a problem, especially when power reaches tens of watts.

The coupler of CPT is composed of four metal plates. Compared with the IPT coupler, the simple structure of the CPT coupler helps to shrink the size of the receiver, which helps to reduce the design complexity and cost. It does not need magnetic shieling layer, thus is cheap, thin and not fragile. Moreover, CPT also has advantages like low standby power loss (when there is no receiver, there is no primary current) [11], capable of transferring power through metal objects [12] and low electromagnetic interference (EMI) [13]. However, CPT method suffers from low coupling capacitance problem and thus is not preferred for both research and application at the beginning. Deepak Rozario et.al gave a detailed analysis and design of coupling capacitors for capacitive power transfer [14]. With the improvement of semiconductor technology, wide-band-gap devices like GaN mosfets can realize nearly 100MHz switching frequency with power up to 100W. Liang Huang et.al researched the autonomous current-fed push-pull converter and class E converter for megahertz capacitive power transfer and their difference [15]. These researches shade new light to the using of CPT for low power consumer electronics. Another fatal problem of CPT system is that the coupling capacitor formed by transmitter pad and receiver pad changes dramatically when the conditions around these pads change. For example, in the laptop application, the vibration and deformation of the receiver resulted from the user's operation will lead to the change of the coupling capacitance, which will thus changes the resonant frequency. One solution is to track the real-time resonant frequency by modifying the switching frequency. However, the tracking of resonant frequency is not precise and the switching frequency is easily to fall outside the range of ISM standard (6.765-6.795MHz). As a result, pure CPT is not practical in such kind of applications. A complicated compensation network [16] can be used to reduce the gain fluctuation caused by the capacitance

variation. However, additional inductors and capacitors are needed, which will weaken CPT's advantages in terms of simplicity, high power density and low cost.

To utilize the advantages of both IPT and CPT, hybrid wireless power transfer concept has been proposed and investigated by researchers. A 2.84kW inductive and capacitive combined wireless power transfer system with 94.5% efficiency over 150 mm distance for EV charging is demonstrated in [17]. But the RMS voltage between the capacitive coupler is as high as 3.4 kV. Thus, the safety problem is a key concern. An inductive and capacitive integrated coupler and a 100W prototype with 73.6% efficiency over 18mm distance is presented in [18]. The inductive coupler and capacitive coupler are integrated together as a single coupler. However, its power density is relatively low considering the size of the integrated coupler (468mm x 468mm x 36mm). Similar hybrid concept is also used in DC/DC research to increase power density. A hybrid converter topology called "MagCap" which uses inductive power transfer and capacitive power transfer at the same time is presented in [19]. A bidirectional DC-DC converter with both magnetic path and capacitor path is built with the benefit of higher power density.

In this paper, a novel hybrid coupler is proposed and designed with the aim of keeping a stable open-loop gain when coupling capacitance varies. The physical structure and working principle of the proposed hybrid coupler is introduced firstly and followed by design considerations of the coupler. An in-depth mathematical evaluation and comparison of the gain characteristics of IPT, CPT and the proposed hybrid coupler is given. Compared with CPT, the open loop gain variation of the proposed hybrid coupler is reduced from 92.68% to 16.27%, which ensures a stable output voltage when coupling capacitance changes. A stable gain variation is also benefit for the control loop design.

This paper is organized as follows. The physical structure and working principle of the hybrid coupler is introduced in section II. In section III, the parameters that affect the coupling capacitance and the coil inductance is analysed and calculated. The open loop gains of inductive, capacitive and hybrid coupler are derived in section IV. A simplified design guideline is given in section V. The simulation and experimental results of a 40W prototype are given in section VI. The waveform, charging robustness of inductive coupler, capacitive coupler, and the proposed hybrid coupler are demonstrated. Conclusions are given in section VII.

2. Dimension and equivalent circuit of the hybrid coupler

The proposed hybrid coupler is shown in Fig. 1, which is composed of two separable PCB boards, namely the primary pad and secondary pad. The primary pad is connected to the transmitter side inverter and the secondary pad is connected to the receiver side rectifier. Power is transferred wirelessly from the primary pad to secondary pad through both magnetic field (marked as 'B field' in Fig. 1) and electric field (marked as 'E field' in Fig. 1). The

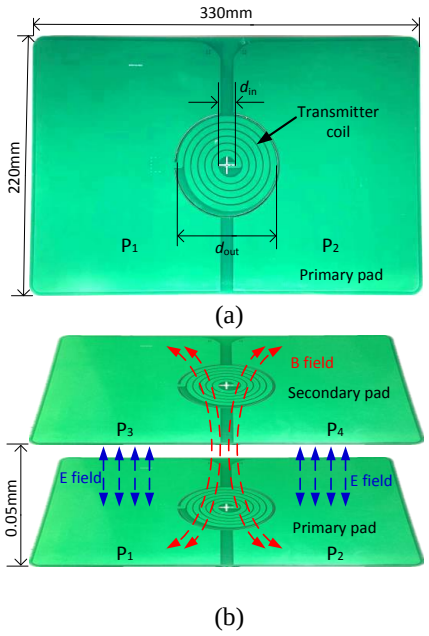

Fig. 1. *Physical structure of the proposed hybrid coupler* ***(a)*** *top view,* ***(b)*** *3D view*

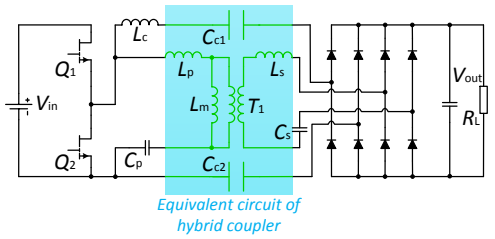

Fig. 2. *Equivalent circuit of the HWPT system*

primary pad including two capacitor plates (P_1 and P_2) and a PCB based coil. The secondary pad also including two capacitor plates (P_3 and P_4) and coil. Dimensions of the hybrid coupler is determined by the bottom size of the receiver according to specific application. For example, a coupler with length of 330mm and width of 220mm is designed for a 14-inches laptop application with some margin around edges. Since the receiver is placed on the table, the vertical distance between the transmitter and the receiver is generally less than 1mm.

To avoid confusion, here we define hybrid wireless power transfer (HWPT) as a system using the proposed hybrid coupler. The HWPT includes an IPT branch and a CPT branch. The topology of the whole HWPT system is shown in Fig. 2. Besides the hybrid coupler, the system is composed of a primary high frequency inverter, two full-bridge rectifier circuits for each branch and a load. The shadowed area in Fig. 2 indicates the equivalent circuit of the proposed hybrid coupler. Each pair of the primary side plates and the secondary side plates can be viewed as a parallel plate capacitor, which is used

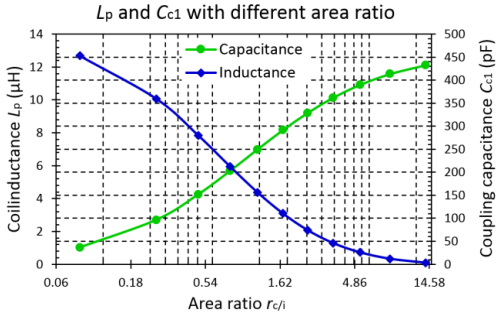

Fig. 3. *Coupling capacitance and coil inductance when area ratio changes*

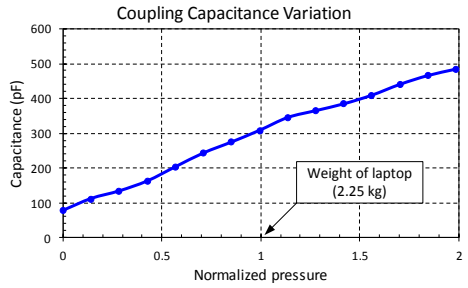

Fig. 4. *Variation of coupling capacitance as a function of pressure on the receiver pad*

for capacitive power transfer. P_1 and P_3 compose C_{c1}; P_2 and P_4 compose C_{c2}. The inductive branch of the hybrid coupler is shown as a transformer circuit with magnetizing inductance L_m, primary leakage inductance L_p, secondary side leakage inductance L_s and an ideal transformer T_1. The CPT branch of the hybrid coupler is equivalent to two capacitors C_{c1} and C_{c2}.

Compensation circuits are needed for both IPT and CPT to suppress the reactive power. In prior-art researches, the topologies of IPT compensation circuit including series compensation, parallel compensation, LCL compensation [20], LCC compensation [21] etc. For CPT, the compensation circuit include series compensation, LC compensation [22], LCL compensation, LCLC compensation [23], CLLC compensation [24] and etc. In this paper, series compensation is used. L_c is the series compensation inductor of the CPT branch; C_p is the primary compensation capacitor and $C_s$is the secondary compensation capacitor for the IPT branch.

To avoid reactive circulating current between the IPT and the CPT branch, two rectifier bridges are used. The output of the rectifiers can be either parallel connected or series connected. If the two rectifiers are parallel connected, the output voltage will be clamped by the one with higher output voltage; if the two rectifiers are series connected, the output current will be the same and the one with lower output voltage will handle lower power [25] [26]. Here, the output of IPT branch and CPT branch are parallel connected to power a single load. At primary side, the CPT branch and IPT branch are parallel connected.

3. Design of hybrid coupler

3.1. Area of capacitor and coil

Although the size of the hybrid coupler is determined by specific application, the area of capacitor and coil or the percentage of their contribution to the whole coupler size can still be designed to ensure the hybrid coupler works in the optimized condition. For simplicity, the hybrid coupler is designed symmetrically, which means the capacitances of C_{c1} and C_{c2} are equal, and the inductances of L_p and L_s are also the same.

$$C = \varepsilon_0 \varepsilon_r \frac{A}{d} \tag{1}$$

As shown in formula (1), it is well known that the coupling capacitance of a parallel plate capacitor is determined by plate area A, relative dielectric constant of the insulation layer ε_r and its thickness d.

For PCB based coil, the coil inductance can be calculated according to empirical formula given by [27],

$$L = \frac{\mu n^2 d_{avg} c_1}{2}\left(\ln\left(c_2/\rho\right) + c_3\rho + c_4\rho^2\right) \tag{2}$$

Where n is number of turns, c_i are layout dependent parameters, for circular coil, c_1 is 1, c_2 equals to 2.46, c_3 equals to zero and c_4 is 0.2; d_{avg} is the average of inner and outer diameter (d_{in} and d_{out}), and ρ is another parameter determined by inner and outer diameter,

$$\begin{cases} d_{avg} = \frac{1}{2}(d_{in} + d_{out}) \\ \rho = (d_{out} - d_{in})/(d_{in} + d_{out}) \end{cases} \tag{3}$$

The width of each turn is determined by d_{in}, d_{out} and number of turns n, the width can be calculated as

$$w = \frac{d_{out} - d_{in} + 2s}{2n} - s \tag{4}$$

Where s is the distance between two turns. For low power applications, since the insolation is not a problem, this distance can be set as low as possible.

Define the area ratio of capacitor plate and coil as

$$r_{c/i} = \frac{A_{cap}}{A_{coil}} = \frac{A_{cap}}{A - A_{cap}} \tag{5}$$

Where A indicates the total area of the hybrid coupler. Then the coupling capacitance and coil inductance as a function of the area ratio is shown as Fig. 3.

As will be explained in the next section, the gain curve of both IPT and CPT is determined by Q value of the resonant tank, as shown in formula (12) and (21). The Q value is affected by the ratio of coupling capacitance and its compensation inductance L_c for CPT (coil inductance and its compensation capacitance C_p for IPT). A high Q value makes the gain curve of CPT or IPT sensitive to system condition changes like load change, which is not desired for control. Thus, the area of coupling capacitor and coil should be determined according to Fig. 3 with the criteria that the Q_1 in (12) equals to Q_2 in (21).

3.2. Coupling capacitance variation

The capacitor design in section 3.1 is based on a precondition that the receiver is put well aligned to the transmitter pad and the pressure between capacitor plates is the normal weight of receiver (e.g. the normal weight of laptop). But working conditions always change when a WPT system is used in real applications. For example, the receiver may not be well aligned to transmitter pad or there may be a piece of paper or dust between transmitter capacitor pads. When a keyboard or laptop is been used (like typing), the coupling capacitance also changes. All these changes in working conditions can be abstracted as the variation of coupling capacitance.

Fig. 4 gives the measured capacitance variation under different working conditions. The measurement is based on a coupler for laptop. It can be inspected that C_c is can change from 70pF to 480pF at different working conditions. As a result, the resonant frequency of CPT will be changed from 5.39MHz to 14.26MHz, which is out of the operating frequency range given in ISM [14].

4. Gain of inductive, capacitive and hybrid coupler

Using fundamental approximation [28], half bridge at the primary side of Fig. 2 can be simplified as a sinusoidal voltage source. The load and the rectifier circuit in Fig. 2 can also be simplified as an equivalent AC resistance

$$R_{ac\_cpt} = \frac{8n}{\pi^2} R_L \tag{6}$$

Where n=1 for full bridge rectifier and n=2 for half bridge rectifier. For the modeling of WPT coupler, there are several theories like mutual inductance theory [29], transformer theory [30] and coupled-mode theory [31]. Each theory is realizable and equivalent substantially. The transformer theory is used in this paper since it is well adopted in power electronics area.

4.1. Gain of CPT

The equivalent circuit of CPT branch is shown as Fig. 5. The resonant frequency of CPT is,

$$f_0 = \frac{1}{2\pi\sqrt{L_c \dfrac{C_{c1}C_{c2}}{C_{c1}+C_{c2}}}} = \frac{1}{2\pi\sqrt{L_c C_c}} \tag{7}$$

Where C_c is the series value of C_{c1} and C_{c2}.

The impedance of CPT seen from voltage source to load is,

$$Z_{cpt} = j\omega L_c + \frac{1}{j\omega C_c} + R_{ac\_cpt} \tag{8}$$

Then the open-loop gain of CPT can be calculated as,

$$G_{CPT}(\omega) = \frac{U_{ac\_cpt}}{U_s} = \frac{R_{ac\_cpt}}{j\omega L_c + \dfrac{1}{j\omega C_c} + R_{ac\_cpt}} \tag{9}$$

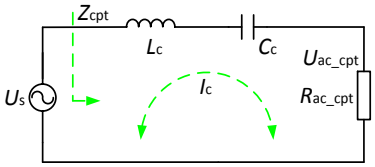

Fig. 5. *Equivalent circuit of capacitive coupler*

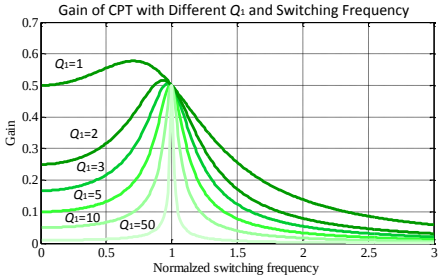

Fig. 6. *Gain of CPT as a function of switching frequency and characteristic impedance (Q_1)*

Where the numerator is the equivalent load resistance and the denominator is the total loop impedance. Since they are series connected, the gain of CPT equals to the ratio of load impedance to the total loop impedance.

Define: 1) Normalized working frequency $f_n = f / f_0$, where f is the actual working frequency, $f = \omega / 2\pi$ and f_0 is the resonant frequency of the resonant tank, which is determined by the value of inductor and capacitor. The normalized working frequency express the deviation of working frequency compared with resonant frequency. Thus, the relationship between ω and f_n is,

$$\omega = f_n / \sqrt{L_c C_c} \tag{10}$$

2) Characteristic impedance Z_0,

$$Z_0 = \sqrt{\frac{L_c}{C_c}} = 2\pi f_0 L_c = \frac{1}{2\pi f_0 C_c} \tag{11}$$

3) Quality factor Q_1,

$$Q_1 = \frac{Z_0}{R_{ac\_cpt}} = \frac{1}{R_{ac\_cpt}}\sqrt{\frac{L_c}{C_c}} \tag{12}$$

Substitute (10), (11), and (12) into (9), the AC gain of CPT is,

$$G_{CPT\_ac}(Q_1, f_n) = \frac{1}{Q_1(1-f_n^2) + j \cdot f_n} \tag{13}$$

The AC gain of CPT is a function of Q_1 and f_n, the modulus of AC gain is,

$$\left|G_{CPT\_dc}(Q_1, f_n)\right| = \frac{1}{2}\frac{1}{\sqrt{f_n^2 + Q_1^2(1-f_n)^2}} \tag{14}$$

Where 1/2 indicates the gain of half bridge. The variation of $|G_{CPT\_dc}(Q_1,f_n)|$ is given in Fig. 6, where the x-axis is

normalized working frequency and *y*-axis is the DC gain. The gain of CPT is in a hump-shape, with its peak value at resonant point and drop when f_n increase or decrease away from resonant point. The gain is 0.5 at the resonant frequency. It can be seen that Q_1 will affect the drop speed of the gain curve. Higher Q_1 leads to faster drop speed.

4.2. Gain of IPT

Similar to CPT, the rectifier circuit and load resistance can also be simplified as an equivalent AC resistance.

There are two resonant tanks for IPT, the L_p, C_p and L_s, C_s, their resonant frequency is,

$$f_p = \frac{1}{2\pi\sqrt{L_p C_p}} \tag{15}$$

$$f_s = \frac{1}{2\pi\sqrt{L_s C_s}} \tag{16}$$

For the sake of simplicity, the primary resonant frequency f_0 is equal to the secondary resonant frequency.

The impedance Z_s seen from the magnetizing inductor to load is

$$Z_s = j\omega L_s + \frac{1}{j\omega C_s} + R_{ac\_ipt} \tag{17}$$

Z_s is in parallel with the magnetizing inductor L_m, the gain of IPT branch is

$$G_{IPT}(\omega) = \frac{U_m}{U_s} \cdot \frac{U_{ac\_ipt}}{U_m} = \frac{\frac{L_m \cdot Z_s}{L_m + Z_s}}{j\omega L_p + \frac{1}{j\omega C_p} + \frac{L_m \cdot Z_s}{L_m + Z_s}} \cdot \frac{R_{ac\_ipt}}{Z_s} \tag{18}$$

where the first fraction is the ratio of voltage on L_m over the input voltage U_s, the second fraction is the ratio of voltage on R_{ac_ipt} over the voltage on L_m. Thus the total gain is the product of the two ratios.

Define: 1) Normalized working frequency $f_n = f / f_0$, where f is the actual working frequency, $f = \omega / 2\pi$ and f_0 is the resonant frequency of the resonant tank, which is determined by the value of inductor and capacitor. The normalized working frequency express the deviation of working frequency compared with resonant frequency. Thus, the relationship between ω and f_n is,

$$\omega = f_n / \sqrt{L_p C_p} \tag{19}$$

2) Characteristic impedance Z_0,

$$Z_0 = \sqrt{\frac{L_p}{C_p}} = 2\pi f_0 L_p = \frac{1}{2\pi f_0 C_p} \tag{20}$$

4) Quality factor Q_2,

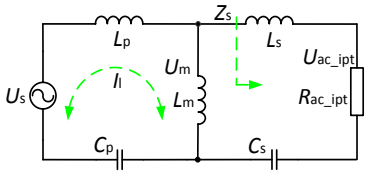

Fig. 7. *Equivalent circuit of inductive coupler*

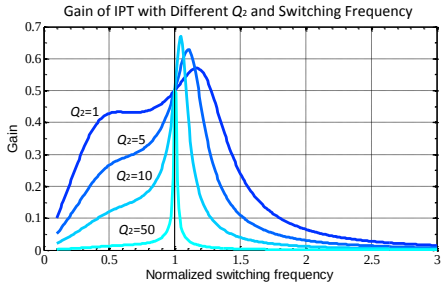

Fig. 8. *Gain of IPT as a function of switching frequency and characteristic impedance (Q_2)*

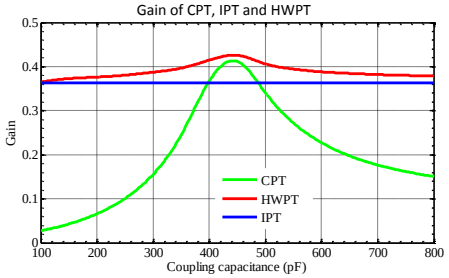

Fig. 9. *Gain of hybrid coupler as a function of coupling capacitance*

$$Q_2 = \frac{Z_0}{R_{ac\_ipt}} = \frac{1}{R_{ac\_ipt}}\sqrt{\frac{L_p}{C_p}} \tag{21}$$

5) Inductor ratio λ,

$$\lambda = L_p / L_m \tag{22}$$

Where L_p is the primary resonant inductor and L_m is the magnetizing inductor.

Substitute (19)-(22) into (18), the AC gain of IPT is,

$$G_{IPT\_ac}(\lambda, Q_2, f_n) = \frac{a + bj}{c + dj} \tag{23}$$

Where

$$a = Q_2(1 - f_n^2) \tag{24}$$

$$b = f_n \tag{25}$$

$$c = (\lambda + Q_2)(1 - f_n^2) \tag{26}$$

$$d = f_n + f_n Q_2 + 2\lambda f_n Q_2 - \frac{\lambda Q_2}{f_n} - f_n^3 Q_2 (1 + \lambda) \tag{27}$$

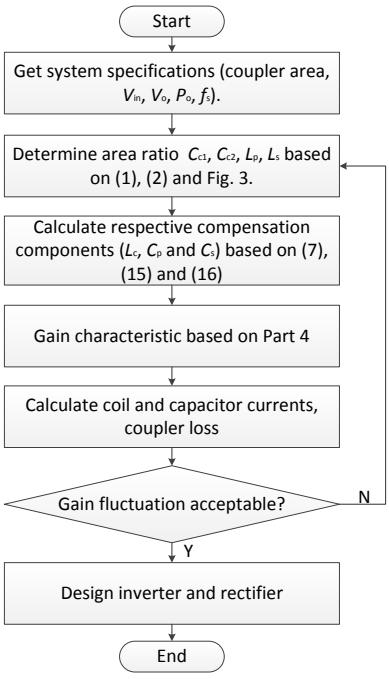

Fig. 10. *Simplified design procedure of a WPT system using proposed hybrid coupler*

The modulus of AC gain is,

$$\left|G_{\text{IPT\_dc}}(\lambda, Q_2, f_n)\right| = \frac{1}{2}\sqrt{\frac{a^2+b^2}{c^2+d^2}} \tag{28}$$

Fig. 8 shows the gain curves with Q_2 changing from 1 to 50. The *x*-axis is normalized working frequency and *y*-axis is the DC gain. The DC gain is fixed to 0.5 at resonant frequency no matter how the Q_2 value changes.

4.3. Gain of HWPT

After getting the DC gain of IPT and CPT, the gain of HWPT system can be derived. According to (12) and (21), quality factor Q is affected by equivalent load resistance. The higher load resistance means lower Q value and higher gain as shown in Fig. 6 and Fig. 8. If the IPT and CPT are parallel connected to power the same load, the equivalent resistance seen by IPT or CPT will be higher than the actual resistance. And the actual resistance is the parallel value of the two equivalent resistances seen by IPT or CPT. If the gain of CPT is not the same as that of IPT, both gains will change and finally come to a steady state where the two gains are equal,

$$\left|G_{\text{CPT\_dc}}(Q_1, f_n)\right| = \left|G_{\text{IPT\_dc}}(\lambda, Q_2, f_n)\right| \tag{29}$$

$$\frac{1}{R_{ac}} = \frac{1}{R_{\text{ac\_ipt}}} + \frac{1}{R_{\text{ac\_cpt}}} \tag{30}$$

Where $R_{\text{ac\_CPT}}$ and $R_{\text{ac\_IPT}}$ are the equivalent resistance seen by IPT and CPT respectively. According to (12) and (21),

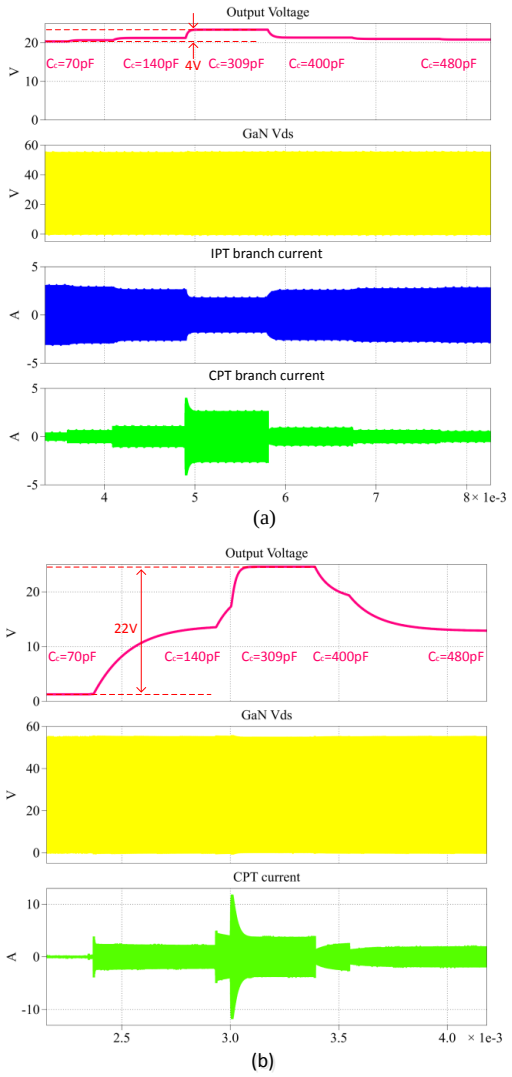

Fig. 11. *Profile of current and output voltage when capacitance changes*
(a) *hybrid coupler when capacitance change from 70pF to 480pF,* ***(b)*** *CPT when capacitance change from 70pF to 480pF*

$$R_{\text{ac\_cpt}} = \frac{1}{Q_1}\sqrt{\frac{L_c}{C_c}}, \quad R_{\text{ac\_ipt}} = \frac{1}{Q_2}\sqrt{\frac{L_p}{C_p}} \tag{31}$$

By solving (27) - (30) to get the Q_1, Q_2. Substituting Q_1 into (14) (or Q_2 into (28)) the final gain of HWPT system is,

$$\left|G_{\text{HWPT}}\right| = \frac{f_n(f_n^3 + \sqrt{\varphi_1})(f_n+1)}{(f_n-1)\cdot\varphi_2} \tag{32}$$

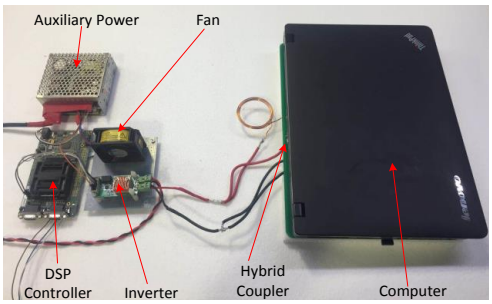

Fig. 12. *Prototype of HWPT system*

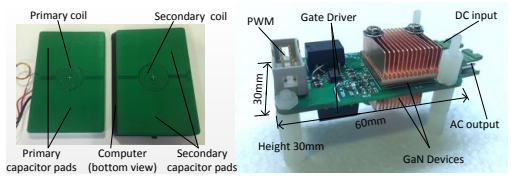

Fig. 13. *Structure of (a) the hybrid coupler and (b) GaN half bridge inverter*

Table 1 Simulation and experimental parameters

Symbol	Value	Symbol	Value
L_p, L_s	0.75μH	f_{cpt}	5.4-10.1MHz
C_p, C_s	850pF	GaN	GS61004B
L_m	1.04μH	Diode	VSSC8L45
f_{ipt}	6.30MHz	R_L	10Ω
L_c	1.78μH	f_{sw}	6.78MHz
C_{c1}, C_{c2}	140-960pF	P_o	40W

Where

$$\varphi_1 = (-\lambda^4 - 2\lambda^3 - \lambda^2) f_n^{\,8} + (4\lambda^4 + 6\lambda^3 + \lambda^2 + 1) f_n^{\,6} + (2\lambda^2 - 6\lambda^3 - 6\lambda^4) f_n^{\,4} - 2\lambda^2 f_n^{\,3} + (4\lambda^4 + 2\lambda^3) f_n^{\,2} - \lambda^4$$

$$\varphi_2 = (\lambda + 1)^2 f_n^{\,6} + 2(\lambda + 1)^2 f_n^{\,5} + (2 - \lambda^2) f_n^{\,4} + (2 - 4\lambda - 4\lambda^2) f_n^{\,3} - (\lambda^2 + 2\lambda) f_n^{\,2} + 2\lambda^2 f_n + \lambda^2 .$$

The analytical calculation of (32) is quite complicated, but it is possible to solve them using mathematical software, such as Mathcad. Fig. 9 gives the gain of hybrid coupler as a function of coupling capacitance. The gain of independent IPT is not affected by the coupling capacitance of CPT thus it is constant. The gain of CPT is one of the curves of Fig. 6, it firstly increases and then decreases when coupling capacitor changes. If the two systems are parallel connected to combine a HWPT system, the gain of HWPT becomes the red curve in Fig. 9. It varies from 0.36 to 0.43 (16.27%) while the gain of individual CPT system varies from 0.03 to 0.41 (92.68%). It can be seen that the gain (as well as output voltage) of the HWPT is much less sensitive to that of conventional CPT.

5. Simplified design guideline

Based on the analysis from section 2 to 4, the design procedure of a WPT system using proposed hybrid can be summarized as Fig. 10. First, some boundary conditions like input voltage, output voltage, output power, total

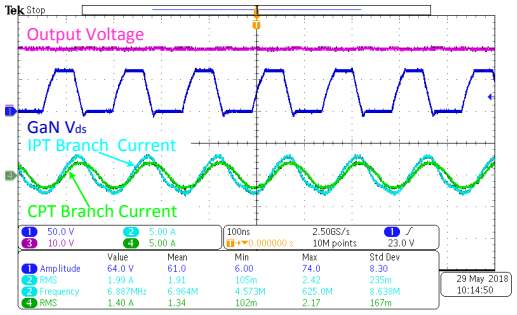

Fig. 14. *Measured output voltage, GaN Drain-Source voltage, IPT branch current and CPT branch current of the hybrid coupler*

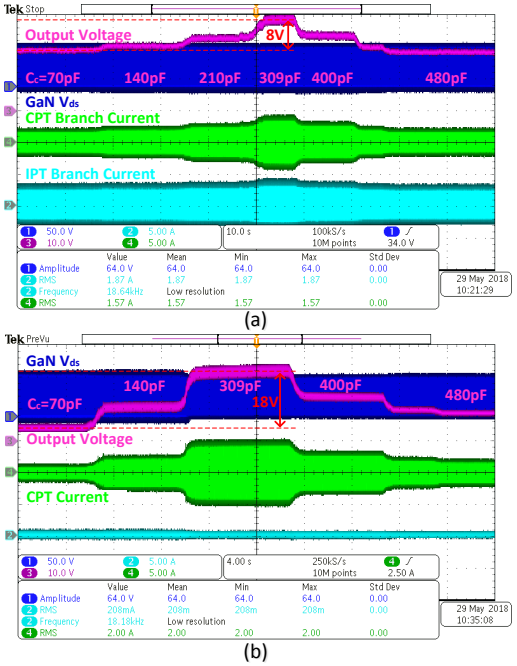

Fig. 15. *Profile of current and output voltage when capacitance changes*

(a)*HWPT system when capacitance change from 70pF to 480pF,* ***(b)*** *Conventional CPT system when capacitance change from 70pF to 480pF*

coupler area and switching frequency is defined by specific application. Then the main parameters of the hybrid coupler are designed according to formula (1), (2) and Fig. 3.

In the third step, components for compensation are designed according to (7), (15) and (16). The gain characteristics of the hybrid coupler should be evaluated to make sure the output voltage and power meets the design requirement under different conditions. If the gain fluctuation requirement is not satisfied, a modification of coil and capacitance should be made and the whole design process be repeated. If the gain fluctuation requirement is

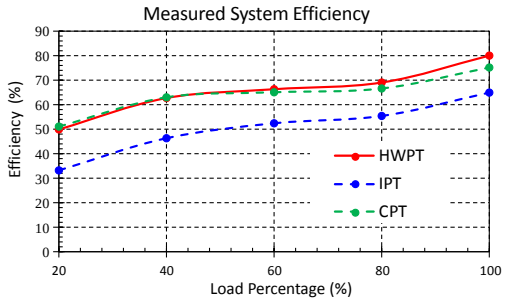

Fig. 16. *Measured efficiency of HWPT, CPT and IPT at different power, from 20% load to 100% load*

satisfied, the coil currents and capacitor currents can be calculated since all the circuit parameters, the input source and load are known at this step. These currents will be used as reference of designing primary inverter and rectifier. As the design of 6.78MHz inverter [8][9] and rectifier [32] has been well researched in previous research, no more description will be repeated in this paper.

6. Simulation and experimental verification

6.1. Simulation

To verify the gain property of the proposed hybrid coupler, simulations have been run in PLECS. The simulation parameters are listed in Table 1. By changing the values of Cc, the resonant frequency as well as the gain of CPT can be changed.

Fig. 11(a) shows the output voltage profile of HWPT system when C_{c1} and C_{c2} changes. A comparison with conventional CPT is also given in Fig. 11(b). For CPT, the output voltage is 24V at normal condition, but drops to 2V when C_c is 70pF and drops to 13V in another direction when C_c is 480pF. The voltage fluctuation range is 22V. For the hybrid coupler, however, the output voltage keeps higher than 20V when capacitance changes and the voltage fluctuation is less than 4V.

6.2. Experimental verification

To further evaluate the performance of the proposed hybrid coupler, a prototype has been built and tested as shown in Fig. 12 and Fig. 13. In Fig. 12, the testing setup includes a GaN based half-bridge inverter, a digital controller (TMS320F28335), a fan, an auxiliary power supply and a hybrid coupler.

The hybrid coupler, shown in Fig. 13(a), is under the computer with an area of 220mm×330mm and thickness of 3.2mm, where 220mm×330mm is the size of laptop and 3.2mm is the thickness of two standard PCB board (primary and secondary), the thickness can be reduced and integrated to laptop and the surface of table. The capacitor plates are formed by the polygon copper layer of PCB. A GaN half-bridge is designed as primary inverter and the switching frequency is set to be 6.78MHz as shown in Fig. 13(b). The size of the inverter is 6cm×3cm×3cm and the two GaN devices are mounted at the same position on both sides of the PCB to minimize the stray inductance. At secondary side, Schottky diodes are using in the rectifier circuit. The components used in the prototype are listed in Table 1. The values are consistent with the simulation parameters.

Fig. 14 shows the measured waveforms of the prototype. The output voltage is regulated to 20V by a DC/DC converter to meet the charging-requirements of laptop. The curve in channel 1 is the measured drain-source voltage of GaN FET of the primary inverter, the V_{ds} drop below zero before they are switched on, thus a soft turn on is reached. The bottom two curves are the currents of IPT branch and CPT branch. Both of them are nearly sinusoidal with some distortion probably caused by the output capacitance of GaN FETs and the junction capacitance of rectifier diodes. This will be further researched and optimized in the future work. It can also be found that the current in the IPT branch and CPT branch are balanced, which means each branch transfers about half of the total power. By using hybrid coupler, the magnetic flux density is lower than pure IPT with the same amount of power transferred.

To study the open-loop gain of the proposed coupler, In Fig. 15, the primary inverter is operated in open-loop mode with 50% duty-cycle. The output DC/DC converter is bypassed and a 10Ω load resistor is connected. Both the proposed hybrid coupler and conventional CPT are tested with coupling capacitance varies from 70pF to 480pF. Fig. 15(a) shows the measured output voltage of hybrid coupler and Fig. 15(b) shows that of CPT. For CPT, the output voltage is 22V at normal condition, but drops to 4V when C_c is 70pF and drops to 12V in another direction when C_c increase to 480pF. The voltage fluctuation range is 18V. For HWPT, the output voltage keeps higher than 20V when capacitance changes, the highest output voltage is about 28V when C_c is 309pF and the voltage fluctuation is less than 8V. The experiment results are well aligned with the simulation results shown in Fig. 11.

Fig. 16 shows the measured efficiency of HWPT system (using proposed hybrid coupler) and conventional IPT, CPT. The efficiency of HWPT is higher than IPT and CPT throughout the load range. The reason is two power transfer paths are used instead of only one for IPT of CPT. The hybrid coupler takes full advantage of the bottom area of receiver device, each branch only needs to handle half of the transferred power and thus coupler losses are reduced. The peak efficiency of the proposed HWPT is 80.02% at 40W output which is higher than CPT, 75.16%, and IPT, 64.93%.

7. Conclusion

A hybrid coupler with stable open-loop gain is proposed, studied and experimentally demonstrated in this paper. Compared with CPT, the proposed hybrid coupler reduces the output voltage fluctuation which reduce the stress on voltage regulation of the second stage DC/DC converter. Compared with IPT, the system efficiency is increased. A detailed derivation is given to theoretically validate the proposed coupler followed by a simplified design guideline. PLECS simulation as well as a 40W, 6.78 MHz experimental prototype for wireless charging of laptop are implemented. The output power of the hybrid coupler maintains higher than 40W when the coupling

capacitance changes from 70pF to 480pF and the output voltage fluctuation is less than 8V while the conventional CPT system is 18V. The system efficiency of HWPT is 80.02% at 40W output, higher than both IPT (64.93%) and CPT (75.16%). The proposed hybrid coupler is suitable for robust and efficient wireless charging of low power electronic products like laptop and tablet.

8. References

[1] Musavi, F., Eberle, W.: 'Overview of wireless power transfer technologies for electric vehicle battery charging', IET Power Electronics., 2014, 7, (1), pp. 60-66

[2] Hui, S. Y. R., Zhong, W., Lee, C. K.: 'A critical review of recent progress in mid-range wireless power transfer', IEEE Trans. Power Electron., 2014, 29, (9), pp. 4500-4511

[3] Wang, G., Liu, W., Sivaprakasam, M., et al.: 'Design and analysis of an adaptive transcutaneous power telemetry for biomedical implants', IEEE Trans Circuits Syst., 2005, 52, (10), pp. 2109-2117

[4] Rozario, D., Azeez, N.A., Williamsoan, S.S.: 'Comprehensive review and comparative analysis of compensation networks for capacitive power transfer systems'. Proc. IEEE 25th Int Symp. Ind. Electron, 2016, pp. 823-829

[5] Zhang, H., Lu, F., Hofmann, H., et al.: 'A 4-plate compact capacitive coupler design and lcl-compensated topology for capacitive power transfer in electric vehicle charging applications', IEEE Trans. Power Electron., 2016, 31, (12), pp. 8541-8551

[6] Lu K., Nguang, S. K., Ji, S., et al.: 'Design of auto frequency tuning capacitive power transfer system based on class-E 2 dc/dc converter', IET Power Electronics., 2017, 10(12), pp. 1588-1595

[7] 'Qi' standard of wireless power consortium, https://www.wirelesspowerconsortium.com/, accessed 10 November 2018

[8] 'A4WP' standard of AirFuel Alliance, https://www.airfuel.org/, accessed 10 November 2018

[9] 'ISM band', https://en.wikipedia.org/wiki/ISM _band, accessed 10 November 2018

[10] Chen, W., Chinga, R. A., Yoshida, S., et al.: 'A 25.6 W 13.56 MHz wireless power transfer system with a 94% efficiency GaN class-E power amplifier'. Proc. IEEE MTTS International, 2012, pp.1-3

[11] Kitabayashi, T., Funato, H., Haruna, J.: 'Loss analysis and power improvement of non-resonant type capacitive power transfer system with three-level operation'. Proc. IEEE ECCE Asia, 2015, PP. 1678-1683

[12] Oruganti, S. K., Heo, S. H., Ma, H., et al.: 'Wireless energy transfer-based transceiver systems for power and/or high-data rate transmission through thick metal walls using sheet-like waveguides', Electronics Letters., 2014, 50, (12), pp. 886-888

[13] Obayashi, S., Tsukahara, H.: 'EMC issues on wireless power transfer'. Proc. IEEE ISEC, 2014, PP.601-604

[14] Rozario, D., Azeez, N. A., Williamson, S. S.: 'Analysis and design of coupling capacitors for contactless capacitive power transfer systems'. Proc. IEEE TECE, 2016, PP.1-7

[15] Huang, L., Hu, A. P., Swain, A.: 'Comparison of two high frequency converters for capacitive power transfer'. Proc. IEEE ECCE, 2014, PP. 5437-5443

[16] Fei, Lu., Zhang, H., Hofmann, H., et al.: 'A dynamic capacitive power transfer system with reduced power pulsation'. Proc. IEEE PELS Workshop, 2016, PP. 60-64

[17] Fei, Lu., Zhang, H., Hofmann, H., et al.: 'An inductive and capacitive combined wireless power transfer system with LC-compensated topology', IEEE Trans. Power Electron., 2016, 31, (12), pp. 8471-8482

[18] Fei, Lu., Zhang, H., Hofmann, H., et al.: 'An inductive and capacitive integrated coupler and its LCL compensation circuit design for wireless power transfer', IEEE Trans. Ind. Appl., 2017, 53, (5), pp. 4903 – 4913

[19] Ishigaki, M., Shin, J., Dede, E. M.: 'A novel soft switching bidirectional DC–DC converter using magnetic and capacitive hybrid power transfer', IEEE Trans. Power Electron., 2017, 32, (9), pp. 6961-6970

[20] Liu, C., Ge, S., Guo, Y., et al.: 'Double-LCL resonant compensation network for electric vehicles wireless power transfer: experimental study and analysis', IET Power Electronics., 2016, 9, (11), pp. 2262-2270

[21] Li, S., Li, W., Deng, J., et al.: 'A double-sided LCC compensation network and its tuning method for wireless power transfer', IEEE Trans. Veh. Technol., 2015, 64, (6), pp. 2261-2273

[22] Fei, Lu., Zhang, H., Hofmann, H., et al.: 'An LCcompensated electric field repeater for long-distance capacitive power transfer', IEEE Trans. Ind. Appl., 2017, 53,(5), pp. 4914 - 4922

[23] Fei, Lu., Zhang, H., Hofmann, H., et al.: 'A doublesided LCLC-compensated capacitive power transfer system for electric vehicle charging', IEEE Trans. Power Electron., 2015, 30, (11), pp. 6011-6014

[24] Fei, Lu., Zhang, H., Hofmann, H., et al.: 'A CLLCcompensated high power and large air-gap capacitive power transfer system for electric vehicle charging applications'. Proc. IEEE APEC, 2016, pp. 1721-1725

[25] Kundu, U., Sensarma, P.: 'Gain-Relationship-Based Automatic Resonant Frequency Tracking in Parallel LLC

Converter', IEEE Trans. Ind. Electron., 2016, 63, (2), pp.874-883

[26] Chen, H., Wu, X., Peng, F., et al.: 'Current balance method for the two-phase interleaved LLC-RDCX with parallel PWM output regulation'. Proc. IEEE PEAC, 2016, PP. 136-141

[27] Mohan, S. S., Del, M. M. H., Boyd S. P.: 'Simple Accurate Expressions for Planar Spiral Inductances', IEEE J. Solid-State Circuit., 1999, 34, (10), PP.1419-1424

[28] Hua, C. C., Fang, Y. H., Lin, C. W.: 'LLC resonant converter for electric vehicle battery chargers', IET Power Electronics., 2016, 9, (12), pp. 2369-2376

[29] Acero, J., Carretero, C., Lope, I., et al.: 'Analysis of the mutual inductance of planar-lumped inductive power transfer systems', IEEE Trans. Power Electron., 2013, 60, (1), pp.410-420

[30] Cheng. Z., Lei. Y., Song. K.: 'Design and Loss Analysis of Loosely Coupled Transformer for an Underwater HighPower Inductive Power Transfer System', IEEE Trans Magnetic., 2015, 51, (7), pp.1-10

[31] Kurs, A., Karalis, A., Moffatt, R.: 'Wireless power transfer via strongly coupled magnetic resonances', Science., 2007, 317, pp.83-86

[32] Liu, M., Fu, M., Ma, C.: 'Low-harmonic-contents and high-efficiency Class E full-wave current-driven rectifier for megahertz wireless power transfer systems', IEEE Trans Power Electron., 2017, 32, (2), pp.1198-1209